Chemistry & Biology, Vol. 12, 279–285, March, 2005, ©2005 Elsevier Ltd All rights reserved. DOI 10.1016/j.chembiol.2005.01.005

Conversion of the Monomeric Red Fluorescent Protein into a Photoactivatable Probe

Brief Communication

Vladislav V. Verkhusha* and Alexander Sorkin
Department of Pharmacology
University of Colorado Health Sciences Center
Box 6511, Mail Stop 8303
Aurora, Colorado 80045

Summary

Photoactivatable fluorescent proteins bring new dimension to the analysis of protein dynamics in the cell. Protein tagged with a photoactivatable label can be visualized and tracked in a spatially and temporally defined manner. Here, we describe a basic rational design strategy to develop monomeric photoactivatable proteins using site-specific mutagenesis of common monomeric red-shifted fluorescent proteins. This strategy was applied to mRFP1, which was converted into probes that are photoactivated by either green or violet light. The latter photoactivatable variants, named PA-mRFP1s, exhibited a 70-fold increase of fluorescence intensity resulting from the photoconversion of a violet-light-absorbing precursor. Detailed characterization of PA-mRFP1s was performed with the purified proteins and the proteins expressed in mammalian cells where the photoactivatable properties were preserved. PA-mRFP1s were used as protein tags to study the intracellular dynamics of GTPase Rab5.

Introduction

Genetically encoded fusions of cellular proteins with GFP and its homologs have been indispensable tools in cell biology [1]. Recently, a new methodology began to emerge with the development of photoactivatable green fluorescent proteins PA-GFP [2], PS-CFP [3], and Dronpa [4] as well as photoactivatable red fluorescent proteins Kaede [5] and kindling fluorescent protein (KFP) [6, 7]. However, only green PA-GFP, PS-CFP, and Dronpa are monomeric and therefore can be applied to protein labeling and tracking. The obligate tetrameric state of red Kaede and KFP limits their application as protein tags, because tetramerization of fluorescent proteins (FPs) causes abnormal localization and function of the tagged partners. A straightforward strategy of FP monomerization consists of two steps repeated several times: (1) site-directed substitutions to disrupt tetramer interfaces, which usually lead to significant decrease of the fluorescence, and (2) rescue of the fluorescence properties by random mutagenesis. This strategy was successfully used to convert tetrameric DsRed into monomeric mRFP1 [8].

We and others previously analyzed the color transitions achieved by mutagenesis and determined the corresponding crucial amino acid positions for tetrameric FPs and nonfluorescent chromoproteins [1, 7]. The analysis based on the GFP [9] and DsRed [10] crystal structures indicated that residues situated spatially close to the chromophore, such as 146, 161, and 197 (numbering is according to DsRed [11]), appear to be the main molecular photoconversion determinants for tetrameric FPs. We therefore hypothesized that the respective mutagenesis of monomeric mRFP1 may directly convert it to photoactivatable red probes suitable for protein tagging.

Results and Discussion

Generation of Photoactivatable Variants

We performed a random saturated mutagenesis of mRFP1 at positions 146, 161, and 197. The library of about 10^4 mutants was visually screened with an epifluorescence microscope. About 10% of the mutants exhibited a photoactivation either by intense green light (CY3 filter) or by intense violet light (DAPI filter). Because photoactivation in the same wavelength range as the chromophore excitation could complicate cellular applications, we further concentrated on characterization of the mutants activatable by violet light. Among various mutants (summarized in Table S1), three variants, mRFP1/S146H/I161V/I197H, mRFP1/S146H/I161C/I197H, and mRFP1/S146H/I161S/I197H (named PA-mRFP1-1, PA-mRFP1-2, and PA-mRFP1-3, respectively) exhibited the highest contrast and the longest lifetime for the fluorescence state after DAPI photoactivation. PA-mRFP1-1 had a slightly higher quantum yield (0.08 versus 0.07 for PA-mRFP1-2 and 0.06 for PA-mRFP1-3). Hence, we present data for the PA-mRFP1-1 variant; however, two other PA-mRFP1 variants exhibited the same spectral, biochemical, and photochemical properties.

Spectral and Biophysical Characterization

Photoactivation of PA-mRFP1-1 for 25 min with a 100 W mercury lamp at 340–380 nm resulted in a 70-fold increase of red fluorescence with excitation and emission maxima at 578 nm and 605 nm, respectively (Figure 1A). PA-mRFP1-1 also preserved its photoactivation properties in the polyacrylamide gel (Figure 1A, inset). The increase of the fluorescence intensity and the quantum yield of the photoactivated PA-mRFP1-1 were similar to that observed for KFP [6]. The increase in the absorbance peak was 20-fold, and the extinction coefficient in the photoactivated state reached 10,000 $M^{-1}cm^{-1}$ (Figure 1B). The photoactivated state was unstable with characteristic lifetimes of 9, 30, and 85 hr at 37°C, 25°C, and 4°C, respectively (Figure S1), indicating that some conformational protein changes occurred during the postactivation period.

The reversibility of the photoactivation and its dependence on temperature has been previously observed for KFP [6]. The residues at positions 146, 161, and 197 in the photoactivatable mRFP1 mutants (Table S1) are similar to those found in several KFP variants [7]. The

*Correspondence: vladislav.verkhusha@uchsc.edu

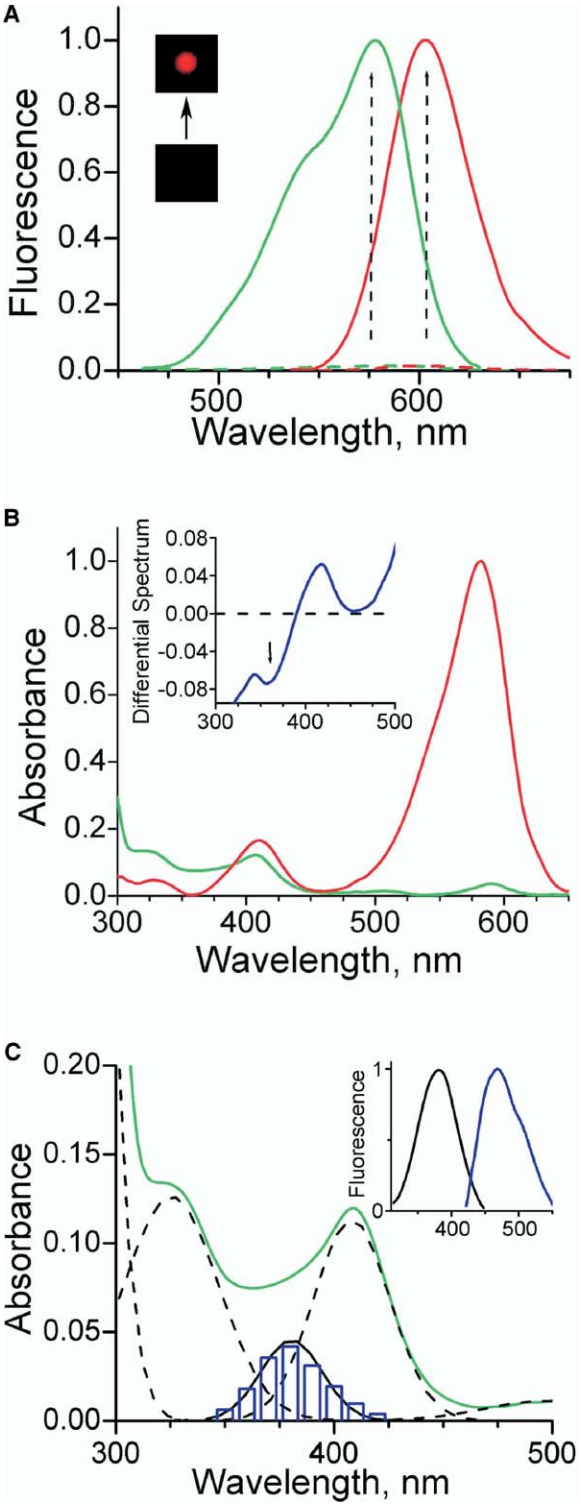

Figure 1. Spectroscopic Properties of PA-mRFP1-1

(A) Excitation (green lines) and emission (red lines) spectra of PA-mRFP1-1 before (dashed lines) and after (solid lines) photoactivation with a 100 W mercury lamp through the 340–380 nm filter for 25 min. Arrows indicate the fluorescence increase. Inset shows a red fluorescent spot resulting from the photoactivation of PA-mRFP1-1 embedded in 15% polyacrylamide gel at 1 mg/ml through a 10× objective.

close properties of the mRFP1 and KFP mutants suggest that the photoactivation mechanism of PA-mRFP1-1 might be also similar to that described for KFP [7]. This mechanism may involve a reversible *cis-trans* chromophore isomerization resulting in the transition from nonfluorescent (*trans*) to fluorescent (*cis*) states, where the chromophore is stabilized through interactions with residues 161 and 146, respectively.

In the fluorescent state, the PA-mRFP1-1 chromophore might be further stabilized through a mechanism suggested for GFP [12] and PA-GFP [2] whereby chromophore conjugation causes charge delocalization to the carbonyl group of Tyr65 instead of the phenolate during the photoconversion. This delocalization is followed by the anionic chromophore stabilization via interaction with side chains such as Arg95. Interestingly, among the PA-GFP variants and the mRFP1 mutants, the highest photoactivation contrast has been achieved in mutants with His146 and His197 substitutions, indicating that the histidines may have the strongest interaction with the chromophore in the photoactivated state. Residues at these positions have been shown to contact the chromophore in GFP and DsRed structures [9, 10]. Remarkably, His197 is also conserved among the KFP variants [7]. On the other hand, the PA-mRFP1-1 chromophore is possibly less stabilized in the photoactivated state than the PA-GFP chromophore because one of the key stabilizing residues, Gln93 [12], is replaced with the conserved Trp93 in the red-shifted proteins including PA-mRFP1-1 and KFP variants.

Before photoactivation, PA-mRFP1-1 had a weak absorbance peak at 588 nm and a dim red fluorescence with excitation/emission maxima at 588 nm and 602 nm, respectively. After the photoactivation, a magnitude of the absorbance spectrum below 390 nm significantly reduced (Figure 1B). These data suggest that the PA-mRFP1-1 preparation consists of two species bearing different types of chromophores and that the violet light could cause formation of a bright red chromophore de novo in the species absorbing below 390 nm. Similar properties were documented for Kaede, where a red chromophore formed from the precursor absorbing at 380 nm [5]. Thus, we hypothesize that there is a similar precursor form of PA-mRFP1-1, but this form is masked by the species with neutral GFP-like [9] and mRFP1/DsRed-like [10] chromophores (Figure 1B; see below). The presence of the immature species with GFP-like chromophore has been documented for mRFP1 [8]. A detectable negative shoulder at 365 nm in the

(B) Absorbance spectra of PA-mRFP1-1 before (green line) and after (red line) the photoactivation. The blue line in the inset presents a differential absorbance spectrum. The arrow indicates the detectable negative shoulder corresponding to a Gaussian component of 380–385 nm.

(C) Gaussian decomposition (black lines) of the PA-mRFP1-1 absorbance spectrum (green line) before the photoactivation. The photoactivation action spectrum is presented as a histogram with a column width of 10 nm (blue columns). The action spectrum is normalized to the 380–385 nm Gaussian component (black solid line). Inset shows the excitation (black line) and the emission (blue line) spectra for a weak PA-mRFP1-1 cyan fluorescence before the photoactivation peaked at 384 and 468 nm, respectively.

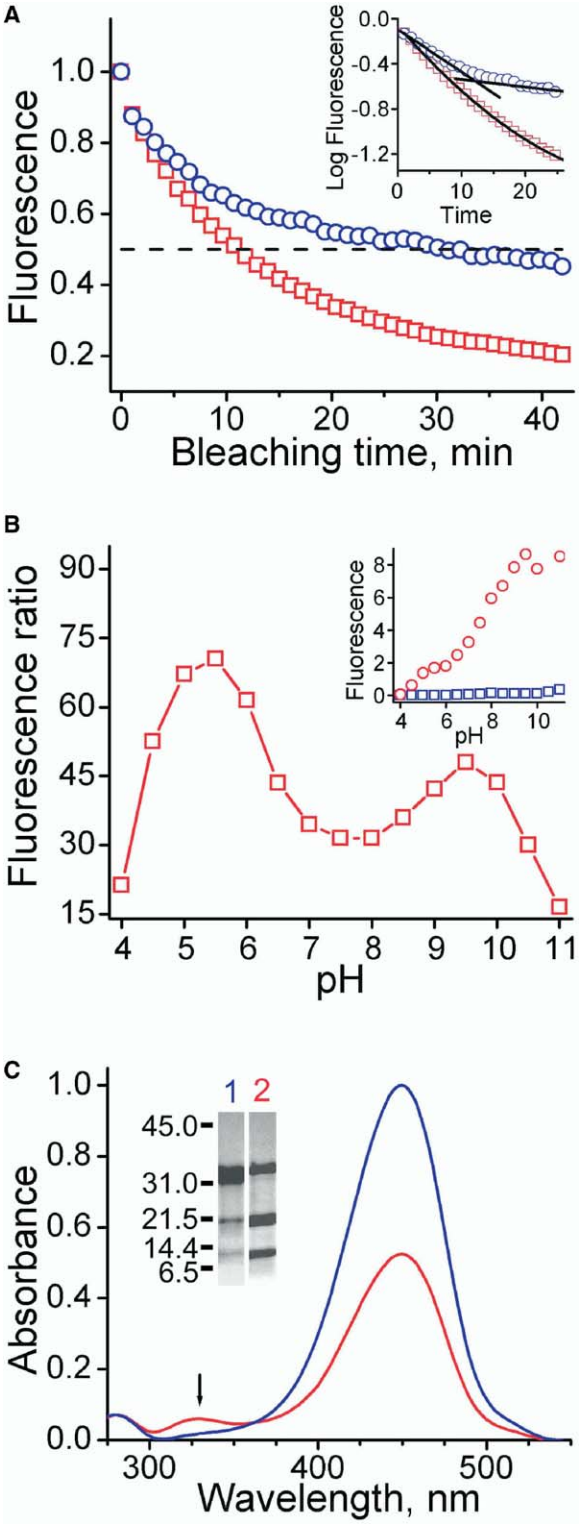

Figure 2. Photochemical and Biochemical Properties of PA-mRFP1-1

(A) Time course of a photobleaching for the photoactivated PA-mRFP1-1 (red squares) and mRFP1 (blue circles) embedded in polyacrylamide gel at 1 mg/ml with a 175 W xenon lamp through the 540–580 nm filter and a 10× objective. Inset shows the exponential fitting of the photobleaching curves in a semilogarithmic scale.

differential absorbance of PA-mRFP1-1 suggested the presence of a spectral component that disappeared after the photoactivation (Figure 1B, inset). Indeed, decomposition of the PA-mRFP1-1 absorbance spectrum before photoactivation into Gaussian peaks revealed a masked component at 380–385 nm (Figure 1C). This peak was absent in the decomposition of the PA-mRFP1-1 spectrum after the photoactivation (data not shown; Figure 1B), indicating that it is the precursor of a photoactivatable red chromophore. This 380–385 nm component exhibited a weak (quantum yield 0.005) cyan fluorescence peak at 468 nm (Figure 1C, inset). The relative increase of the PA-mRFP1-1 red fluorescence after its irradiation with light of varying wavelengths (so-called action spectrum) was further measured. The excitation at 375–385 nm was the most effective in the ability to photoactivate PA-mRFP1-1. Moreover, the action spectrum coincided with the 380–385 nm component (Figure 1C). The degree of photoactivation depended linearly on the intensity of the activation light, indicative of a one-photon process (Figure S2).

Biochemical and Photochemical Properties

PA-mRFP1-1 photobleaching represented a monoexponential process with a characteristic half-time of 11 min, whereas mRFP1 had a two-exponential photobleaching curve (Figure 2A). The value of the characteristic half-time was about one third of an apparent total photobleaching half-time of mRFP1 and was similar to the photobleaching half-time of its fast photobleaching component. These data indicated that photoactivated PA-mRFP1-1 consisted of the homogeneous species, whereas the mRFP1 population consisted minimum of two types of red species, as has been previously suggested [8].

The pH dependencies of PA-mRFP1-1 red fluorescence before and after photoactivation were measured after 10 min of the violet irradiation (100 W mercury lamp). Both emissions significantly increased at acidic pH (Figure 2B, inset). The ratio of fluorescence intensities after and before photobleaching had two peaks, one in the acidic and another in the alkaline region (Figure 2B). The photoactivation contrast at these conditions of photoactivation was 2.2-fold and 1.3-fold higher at the mild-denaturing pH (5.0–5.5 and 9.5–10.0, respectively) as compared to the contrast achieved at the physiological pH (7.0–8.0). The apparent pK_a value was 4.4. Interestingly, the background red fluorescence increased at elevated temperatures (Figure S3) and in the presence of moderate concentrations of chaotropic agents (Figure S4). These data suggested that slight loosening of the PA-mRFP1-1 structure facilitates chro-

(B) Dependence of a fluorescence ratio between the red emission intensities for the photoactivated state (achieved after 10 min irradiation with the 340–380 nm filter and a 10× objective) and the nonfluorescent state from pH value of the sample. Inset shows the absolute values of these photoactivated (red circles) and nonfluorescent (blue squares) intensities.

(C) Absorbance spectra of mRFP1 (blue line) and PA-RFP1-1 (red line) in 1 M NaOH normalized at 280 nm. The arrow indicates 330 nm peak observed in PA-mRFP1 only. Inset shows the denaturing SDS-PAGE gel for mRFP1 (lane 1) and PA-mRFP1-1 (lane 2).

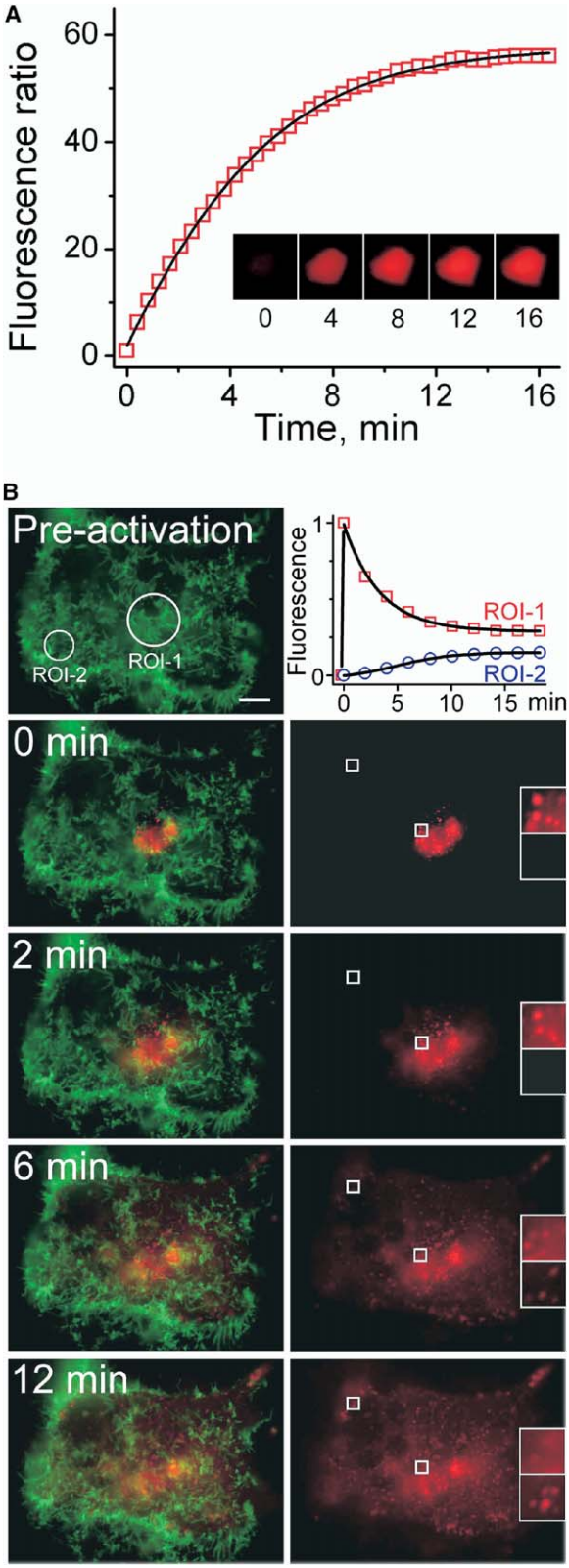

Figure 3. Properties of PA-mRFP1-3 in Living Mammalian Cells

(A) Photoconversion time course of cytoplasmically expressed PA-mRFP1-3 in HEK293 cells irradiated with a 175 W xenon lamp through the 340–380 filter and a 63× objective (red squares). The ordinate axis presents a fluorescence ratio between the total cell intensity at each time point and the total cell intensity at the start of the activation (time zero). The solid black line indicates a mono-exponential fit of the data. Inset shows images of the representative cell excited with the 540–580 nm filter at the times indicated in minutes after the start of photoactivation.

(B) COS-1 cell expressing EYFP-DAT (green channel) and PA-mRFP1-3-Rab5 (red channel) photoactivated with 365 nm dye laser (ROI-1 circle). The PA-mRFP1-3-Rab5 dynamics after the photoactivation (right column) and its overlay with the green channel (left column) are shown at the times indicated. The mean intensities in the red channel in the ROI-1 (red squares) and ROI-2 (blue circles) regions are presented in the top right panel. The intensities are normalized to the mean intensity just after the photoactivation (time zero). Insets in the right column illustrate dynamics of PA-mRFP1-3-Rab5 in the square selections. Bar, 10 μm.

mophore transition from nonfluorescent to the fluorescent state.

It has been suggested that the absorbance spectra of acid- and alkali-denatured FPs can be used to distinguish between their primary chromophore structures [13]. The absorbance of GFP-like chromophore peaks at 384 nm in 1M HCl and at 446 nm in 1M NaOH [14]. Under the same conditions, the DsRed-like chromophore absorbs at 380 and 452 nm, respectively [13, 14]. Acid-denatured mRFP1 and nonactivated PA-mRFP1-1 both exhibited wide absorbance peaks at about 382 nm (not shown). However, the alkali-denatured proteins behaved differently (Figure 2C). The absorbance spectrum of mRFP1 had a wide peak at 450 nm that possibly consisted of the immature species bearing the GFP-like chromophore as well as the mature red species with a DsRed-like chromophore. This observation was consistent with the incomplete maturation of mRFP1 [8]. In contrast, PA-mRFP1-1 had two peaks, at 450 nm and 330 nm. While the former peak consisted of the same GFP-like and DsRed-like chromophores, the latter peak possibly represented the photoactivatable species. The acid- and alkali-denatured spectra of PA-mRFP1-1 did not change after photoactivation. Normalization of mRFP1 and PA-mRFP1-1 spectra at 280 nm indicated that approximately half of PA-mRFP1-1 consisted of the red photoactivatable variant (Figure 2C).

SDS-PAGE analysis further supported this observation. It has been previously reported that mRFP1 exhibited fragmentation into two bands with an apparent mass of 11 kDa (including a polyhistidine tag) and 20 kDa [8] (Figure 2C, inset). This partial cleavage results from a partial hydrolysis of the main-chain acylimine linkage in the DsRed-like chromophore [14]. This fragmentation has never been observed with proteins having GFP-like chromophore. In contrast, more than 50% of PA-mRFP1-1 molecules were cleaved (Figure 2C, inset). The extent of the cleavage was the same for nonactivated and photoactivated PA-mRFP1-1 preparations (not shown). These data suggested that a pool of fragmented PA-mRFP1-1 contained both the bulk of photoactivatable species and a small fraction of the hydrolyzed DsRed/mRFP1-like species. This type of post-translational modification is similar to that observed for KFP and has been shown to be critical for its photoactivatable properties [15].

Expression in Mammalian Cells

To characterize properties of PA-mRFP1s in mammalian cells, these proteins were transiently expressed in HEK293 and COS-1 cell lines. No detectable red fluorescence of expressed PA-mRFP1s was observed before photoactivation. Upon irradiation with the 175 W xenon lamp through the DAPI filter for several minutes or with dye laser (365 nm) for a few seconds, red fluorescence was detected through the CY3 channel (Figure 3A). Interestingly, the PA-mRFP1-3 variant exhibited 60-fold fluorescence contrast in the cytoplasm (Figure 3A). This contrast was significantly higher as compared with the intensity contrasts of PA-mRFP1-1 (25-fold) and PA-mRFP1-2 (35-fold). These data suggested that, similar to the DsRed2 variant, the chromophore formation in PA-mRFP1s was controlled by cell-specific factors [16]. The kinetics of fluorescence increase of PA-mRFP1s was well fitted by a single exponential curve with characteristic times of 4.2–4.5 min, indicative of a first-order photochemical reaction (Figure 3A). Can PA-mRFP1s be used to tag cellular proteins and to visualize spatially defined cellular pools of fusion proteins? The limitation of the use of mRFP1 as a protein tag is related to its spontaneous intracellular aggregation, particularly when it is attached to oligomerizing proteins such as actin, α-tubulin, or caveolin [17] (data not shown). We recently found that mRFP1-fusion of a small GTPase Rab5 does not form aggregates and is fully colocalized with EYFP-Rab5 when is coexpressed [18]. To test the applicability of PA-mRFP1s for protein tagging, a fusion PA-mRFP1-3-Rab5 was prepared. Small GTPases of the Rab family control endosomal biogenesis, fusion, and maturation [19]. Rab5 is located on the cytoplasmic surface of early endosomes and is a key component of a complex responsible for homotypic fusion of early endosomes and cargo sorting [20]. However, very little information is available regarding the dynamics of endosome-cytosol translocations of Rab5 protein and, in fact, of any protein of the Rab subfamily.

PA-mRFP1-3-Rab5 was expressed in COS-1 cells. The cells were also cotransfected with membrane-localizing EYFP-tagged dopamine transporter [21] to facilitate selection of the cellular regions to photoactivate. Local photoactivation of a small region in the perinuclear area using 365 nm laser irradiation resulted in the photoactivation of several endosomes containing PA-mRFP1-3-Rab5 (region of interest ROI-1 of the representative cell in Figure 3B). Time-lapse imaging revealed a gradual decrease of the PA-mRFP1-3-Rab5 fluorescence in the photoactivated region accompanied by the appearance of PA-mRFP1-3-Rab5 fluorescence in other areas. The translocated Rab5 was found both incorporated into endosomes and diffusely distributed in the cytoplasm, presumably in a complex with the guanine nucleotide dissociation inhibitor [22].

The fluorescence intensity of photoactivated PA-mRFP1-3-Rab5 in the ROI-1 was reduced by up to 73% (Figure 3B, top right panel). The time-courses of the fluorescence decrease were fitted by single exponential functions with the half-lives of 3.6-4.4 min for different cells. Interestingly, the time-courses of PA-mRFP1-3-Rab5 translocation out of ROI-1 reached plateau at 25%–28% suggesting that there was an immobile pool of Rab5. The PA-mRFP1-3-Rab5 fluorescence in the peripheral ROI-2 regions increased by up to 15% of the total initial fluorescence intensity of photoactivated ROI-1. In contrast to ROI-1, the fluorescence change in ROI-2 presented sigmoid curves with half-maximal times of 5.1–5.9 min. Changes in the concentrations of PA-mRFP1-3-Rab5 in ROI-1 and ROI-2 could be due to translocation of Rab5 molecules between endosomes through the cytosol, rapid movement of Rab5-labeled endosomes, or formation of Rab5 transport vesicles and their movement. Experiments are underway that should enable us to dissect the dynamics of these processes. Nevertheless, our data demonstrated that PA-mRFP1s can be used to analyze the kinetics of Rab5 trafficking and the assembly of Rab5 microdomains on the endosomal membranes.

Significance

PA-mRFP1 variants represent a first generation of monomeric photoactivatable probes that are distinct from green PA-GFP [2], PS-CFP [3], and Dronpa [4] in terms of red-shifted fluorescence and that can be used for protein labeling and tracking in living cells. We have shown that the residues 146, 161, and 197 appear to be the important molecular determinants for the conversion of monomeric red-shifted FPs, such as mRFP1, into the photoactivatable variants. The rational design strategy for development of photoactivatable probes presented here can be further applied to convert other yellow, orange, or red monomeric FPs [17, 27, 28] and monomeric chromoproteins with red-shifted absorbance [13] into the respective photoactivatable FPs.

Experimental Procedures

Mutagenesis and Screening

Mutagenesis of the pRSETB-mRFP1 plasmid [8] was performed by the overlap-extension method [23]. Colonies of DH5α (Invitrogen) were screened with a Nikon Diaphot 300 microscope equipped with a 100 W mercury lamp, DAPI (340-380 nm), FITC (460-500 nm), and CY3 (540-580 nm) filters (Chroma), and a 10× PlanFluor objective.

Protein Expression and Spectroscopy

Proteins were purified from BL21(DE3) (Stratagene) with Ni-NTA (Qiagen). Photoactivation was performed in a 0.5 cm quartz cuvette (Starna Cells) through a DAPI filter. Absorbance spectra were recorded with a Beckman DU520 Spectrophotometer, and excitation and emission spectra were measured using a PTI Fluorescence Spectrophotometer (Photon Technologies) with protein samples in PBS (pH 7.4) at 25°C. For molar extinction coefficient determination, we relied on estimating mature red chromophore concentrations achieved with denaturation in 1 M NaOH. Based on absorbance of denatured proteins, extinction coefficients for the native state were determined as described [24]. For quantum yield determination, fluorescence of mutants was compared to an equally absorbing amount of DsRed (BD Clontech) (quantum yield 0.70 [25]). Gaussian decomposition and fitting were performed with Origin software (Microcal).

Characterization In Vitro

To study photoactivation under imaging conditions, proteins were embedded at 1 mg/ml in 15% polyacryamide gels immobilized on a glass slide, using cover glasses as spacers [2]. The photoactivation was performed with a Nikon Diaphot 300 microscope. Subsequent imaging or photobleaching was done with *Marianas* workstation (Intelligent Imaging Innovation) based on Zeiss Axiovert 200M

microscope equipped with dual filter wheels, 175 W xenon lamp, 10× Fluar and 63× and 100× oil immersion Plan-Apochromat objectives, CoolSNAP CCD camera (Roper Scientific), DAPI, FITC, and CY3 filters (Chroma), environmental chamber, and controlled by SlideBook 4.0 software. Action spectrum was measured with a Nikon Optiphot microscope equipped with a 175 W xenon lamp, 40× dry Plan-Neofluar objective, and a tunable monochromator on the excitation source with bandwidth of 10 nm. 15% polyacrylamide gels buffered with Hydrion buffers (Micro Essential Laboratory) were used to study pH dependence.

Mammalian Expression

NheI-BsrGI fragments encoding PA-mRFP1s proteins without stop codons were swapped with the EYFP in pEYFP-C1 vector (BD Clontech), resulting in pPA-mRFP1s-C1 plasmids. To generate a plasmid with PA-mRFP1s-Rab5 fusion, the PA-mRFP1s' fragments were swapped with EYFP in pEYFP-Rab5 plasmid [26]. HEK293 and COS-1 cells were cultured in DMEM media (Invitrogen) supplemented with 10% fetal or newborn bovine sera, respectively (Sigma). Cell transfection was performed with Effectene (Qiagen).

Fluorescence Microscopy

Live cell images were acquired with the *Marianas* workstation additionally equipped with Micropoint Ablation 365 nm laser system (Photonic Instruments). A 15 micro Joules laser output was applied for PA-mRFP1s photoactivation in living cells. Total photoactivation time did not exceed 3 s. No detectable changes in cell morphology were observed during this treatment. Adjustment of size and location of the photoactivatable area and quantification of intensities were performed with SlideBook v. 4.0 software.

Supplemental Data

Supplemental Data are available at http://www.chembiol.com/cgi/content/full/12/3/279/DC1/.

Acknowledgments

We thank R. Tsien for cDNA of mRFP1, K. Lukyanov for helpful discussions, and J. Remington for valuable advice. This work was supported by grants from National Institutes of Health AA13489-INIA, GM70358 (V.V.V.), and DA14204 (A.S.).

Received: October 1, 2004
Revised: January 7, 2005
Accepted: January 10, 2005
Published: March 25, 2005

References

1. Verkhusha, V.V., and Lukyanov, K.A. (2004). The molecular properties and applications of Anthozoa fluorescent proteins and chromoproteins. Nat. Biotechnol. *22*, 289–296.
2. Patterson, G.H., and Lippincott-Schwartz, J. (2002). A photoactivatable GFP for selective photolabeling of proteins and cells. Science *13*, 1873–1877.
3. Chudakov, D.M., Verkhusha, V.V., Staroverov, D.B., Souslova, E.A., Lukyanov, S., and Lukyanov, K.A. (2004). Photoswitchable cyan fluorescent protein for protein tracking. Nat. Biotechnol. *22*, 1435–1439.
4. Ando, R., Mizuno, H., and Miyawaki, A. (2004). Regulated fast nucleocytoplasmic shuttling observed by reversible protein highlighting. Science *306*, 1370–1373.
5. Ando, R., Hama, H., Yamamoto-Hino, M., Mizuno, H., and Miyawaki, A. (2002). An optical marker based on the UV-induced green-to-red photoconversion of a fluorescent protein. Proc. Natl. Acad. Sci. USA *99*, 12651–12656.
6. Chudakov, D.M., Belousov, V.V., Zaraisky, A.G., Novoselov, V.V., Staroverov, D.B., Zorov, D.B., Lukyanov, S., and Lukyanov, K.A. (2003). Kindling fluorescent proteins for precise in vivo photolabeling. Nat. Biotechnol. *21*, 191–194.
7. Chudakov, D.M., Feofanov, A.V., Mudrik, N.N., Lukyanov, S., and Lukyanov, K.A. (2003). Chromophore environment provides clue to kindling fluorescent protein riddle. J. Biol. Chem. *278*, 7215–7219.
8. Campbell, R.E., Tour, O., Palmer, A.E., Steinbach, P.A., Baird, G.S., Zacharias, D.A., and Tsien, R.Y. (2002). A monomeric red fluorescent protein. Proc. Natl. Acad. Sci. USA *99*, 7877–7882.
9. Ormo, M., Cubitt, A.B., Kallio, K., Gross, L.A., Tsien, R.Y., and Remington, S.J. (1996). Crystal structure of the Aequorea victoria green fluorescent protein. Science *273*, 1392–1395.
10. Yarbrough, D., Wachter, R.M., Kallio, K., Matz, M.V., and Remington, S.J. (2001). Refined crystal structure of DsRed, a red fluorescent protein from coral, at 2.0-A resolution. Proc. Natl. Acad. Sci. USA *98*, 462–467.
11. Matz, M.V., Fradkov, A.F., Labas, Y.A., Savitsky, A.P., Zaraisky, A.G., Markelov, M.L., and Lukyanov, S.A. (1999). Fluorescent proteins from nonbioluminescent Anthozoa species. Nat. Biotechnol. *17*, 969–973.
12. Prendergast, F.G. (1999). Biophysics of the green fluorescent protein. Methods Cell Biol. *58*, 1–18.
13. Shagin, D.A., Barsova, E.V., Yanushevich, Yu., Fradkov, A., Kulyanov, K.A., Labas, Yu.A., Ugalde, J., Meyer, A., Nunes, J., Widder, E.A., et al. (2004). GFP-like proteins as ubiquitous Metazoan superfamily: evolution of functional features and structural complexity. Mol. Biol. Evol. *21*, 841–850.
14. Gross, L.A., Baird, G.S., Hoffman, R.C., Baldridge, K.K., and Tsien, R.Y. (2000). The structure of the chromophore within DsRed, a red fluorescent protein from coral. Proc. Natl. Acad. Sci. USA *97*, 11990–11995.
15. Wilmann, P.G., Petersen, J., Devenish, R.J., Prescott, M., and Rossjohn, J. (2005). Variations on the GFP chromophore: A polypeptide fragmentation within the chromophore revealed in the 2.1 A crystal structure of a non-fluorescent chromoprotein from Anemonia sulcata. J. Biol. Chem. *280*, 2401–2404.
16. Terskikh, A.V., Fradkov, A.F., Zaraisky, A.G., Kajava, A.V., and Angres, B. (2002). Analysis of DsRed mutants. Space around the fluorophore accelerates fluorescence development. J. Biol. Chem. *277*, 7633–7636.
17. Shaner, N.C., Campbell, R.E., Steinbach, P.A., Giepmans, B.N., Palmer, A.E., and Tsien, R.Y. (2004). Improved monomeric red, orange and yellow fluorescent proteins derived from Discosoma sp. red fluorescent protein. Nat. Biotechnol. *22*, 1567–1572.
18. Galperin, E., Verkhusha, V.V., and Sorkin, A. (2004). Three-chromophore FRET microscopy to analyze multiprotein interactions in living cells. Nat. Methods *1*, 209–217.
19. Zerial, M., and McBride, H. (2001). Rab proteins as membrane organizers. Nat. Rev. Mol. Cell Biol. *2*, 107–117.
20. Stenmark, H., Parton, R.G., Steele-Mortimer, O., Lutcke, A., Gruenberg, J., and Zerial, M. (1994). Inhibition of Rab5 GTPase stimulates membrane fusion in endocytosis. EMBO J. *13*, 1287–1296.
21. Sorkina, T., Doolen, S., Galperin, E., Zahniser, N.R., and Sorkin, A. (2003). Oligomerization of dopamine transporters visualized in living cells by fluorescence resonance energy transfer microscopy. J. Biol. Chem. *278*, 28274–28283.
22. Pfeffer, S.R. (2001). Rab GTPases: specifying and deciphering organelle identity and function. Trends Cell Biol. *11*, 487–491.
23. Ho, S.N., Hunt, H.D., Horton, R.M., Pullen, J.K., and Pease, L.R. (1989). Site-directed mutagenesis by overlap extension using the polymerase chain reaction. Gene *77*, 51–59.
24. Bulina, M.E., Chudakov, D.M., Mudrik, N.N., and Lukyanov, K.A. (2002). Interconversion of Anthozoa GFP-like fluorescent and non-fluorescent proteins by mutagenesis. BMC Biochem. *3*, 7.
25. Baird, G.S., Zacharias, D.A., and Tsien, R.Y. (2000). Biochemistry, mutagenesis, and oligomerization of DsRed, a red fluorescent protein from coral. Proc. Natl. Acad. Sci. USA *97*, 11984–11989.

26. Galperin, E., and Sorkin, A. (2003). Visualization of Rab5 activity in living cells by FRET microscopy and influence of plasma membrane targeted Rab5 on clathrin-dependant endocytosis. J. Cell Sci. *116*, 4799–4810.
27. Karasawa, S., Araki, T., Nagai, T., Mizuno, H., and Miyawaki, A. (2004). Cyan-emitting and orange-emitting fluorescent proteins as a donor/acceptor pair for fluorescence resonance energy transfer. Biochem. J. *381*, 307–312.
28. Wang, L., Jackson, W.C., Steinbach, P.A., and Tsien, R.Y. (2004). Evolution of new nonantibody proteins via iterative somatic hypermutation. Proc. Natl. Acad. Sci. USA *101*, 16745–16749.